

## ORIGINAL ARTICLE

# Colorectal liver metastases that survive radioembolization display features of aggressive tumor behavior

Daan Andel<sup>1</sup>, Jeroen Hagendoorn<sup>1</sup>, Ahmed Aziz Alsultan<sup>2</sup>, Miangela Marie Lacle<sup>3</sup>, Maarten Leonard Johannes Smits<sup>2</sup>, Arthur Johannes Anthonius Theodorus Braat<sup>2</sup>, Onno Kranenburg<sup>1</sup>, Marnix Gerard Ernest Hendrik Lam<sup>2</sup> & Inne Hilbrand Max Borel Rinkes<sup>1</sup>

<sup>1</sup>Department of Surgical Oncology, University Medical Center Utrecht, Cancer Center, Utrecht, the Netherlands, <sup>2</sup>Department of Radiology and Nuclear Medicine, University Medical Center Utrecht, Cancer Center, Utrecht, the Netherlands, and <sup>3</sup>Department of Pathology, University Medical Center Utrecht, Utrecht University, Utrecht, the Netherlands

## Abstract

**Background:** Radiation lobectomy is a therapeutic approach that involves targeted radiation delivery to induce future liver remnant hypertrophy and tumor control. In patients with colorectal liver metastases, only 30–40% have complete tumor regression. The importance of tumor biology in treatment response remains elusive.

**Methods:** Patients with colorectal liver metastases who received radiation lobectomy were selected from surgical pathology files. Using a machine learning scoring protocol, pathological response was correlated to tumor absorbed dose and expression of markers of radioresistance Ki-67 (proliferation), CAIX (hypoxia), Olfm4 (cancer stem cells) and CD45 (leukocytes).

**Results:** No linear association was found between tumor dose and response ( $p < 0.1$ ,  $P = 0.73$  ( $^{90}\text{Y}$ ),  $P = 0.92$  ( $^{166}\text{Ho}$ )). Response did correlate with proliferation ( $p = 0.56$ ,  $P = 0.012$ ), and non-responsive lesions had large pools ( $>15\%$ ) of Olfm4 positive cancer stem cells (Fisher's exact test,  $P = 0.0037$ ). Responding lesions (regression grade  $\leq 2$ ) were highly hypoxic compared to moderate and non-responding lesions ( $P = 0.011$ ). Non-responsive lesions had more tumor-infiltrating leukocytes ( $3240 \text{ cells/mm}^2$  versus  $650 \text{ cells/mm}^2$ ), although this difference was not significant ( $P = 0.08$ ).

**Conclusion:** The aggressive phenotype of a subset of surviving cancer cells emphasizes the importance of prompt resection after radiation lobectomy.

Received 3 March 2023; accepted 20 June 2023

## Correspondence

Daan Andel, PO BOX 85500, 3508 GA, Utrecht, the Netherlands. E-mail: [D.S.H.Andel-3@umcutrecht.nl](mailto:D.S.H.Andel-3@umcutrecht.nl) (D. Andel)

## Correspondence

Inne Hilbrand Max Borel Rinkes, PO BOX 85500, 3508 GA, Utrecht, the Netherlands. E-mail: [I.H.M.BorelRinkes@umcutrecht.nl](mailto:I.H.M.BorelRinkes@umcutrecht.nl) (I.H.M. Borel Rinkes)

## Introduction

Radioembolization has emerged as a valuable palliative treatment option for patients with liver malignancies.<sup>1</sup> Radioembolization uses transarterial infusion of radioactive microspheres to treat tumors locally. When administered in high doses to one lobe, it is called radiation lobectomy.<sup>2</sup> Radiation lobectomy is increasingly used to facilitate surgical resection as it can increase both the volume and function of the non-perfused lobe - termed the future liver remnant (FLR).<sup>3</sup> As such, radiation lobectomy may

reduce the likelihood of post hepatectomy liver failure. Currently available microspheres are yttrium-90 ( $^{90}\text{Y}$ ) (SIR-Spheres®, Sirtex or TheraSphere™, Boston Scientific) microspheres and holmium-166 ( $^{166}\text{Ho}$ ) (QuiremSpheres®, Quirem Medical) microspheres.

The current standard of care for inducing FLR growth is portal vein embolization.<sup>4</sup> Portal vein embolization generally causes satisfactory hypertrophy of the FLR, but does not treat the tumor. Thus, the value of radiation lobectomy is reflected in the fact that

hypertrophy can be induced while simultaneously controlling the tumor.

Complete radiological response of colorectal liver metastases to radioembolization ranges from 30 to 40%.<sup>5</sup> Factors influencing the response to radioembolization include dosage, (heterogeneous) microsphere distribution, pre-treatment mutation status and vascularization.<sup>6–11</sup> More generally, the response to radiation therapy is also influenced by hypoxia, antitumor immunity and the presence of radiation-resistant cancer stem cells.<sup>12–15</sup> To this date, the histological biology of radioembolization-surviving tumor cells has not been studied, possibly due to the scarcity of resection material. The aim of this pilot study was to characterize the inter- and intratumor response to radioembolization/radiation lobectomy and the relationship with immunohistochemical markers of radiation resistance Ki-67 (proliferation), CAIX (hypoxia), Olfm4 (colorectal cancer stem cells) and CD45 (leukocytes).

## Patients and methods

### Case selection

A retrospective review of all patients with colorectal liver metastases who received radioembolization/radiation lobectomy prior to surgical hepatectomy from 2014 to 2021 at the University Medical Center Utrecht (Anonymized), was conducted. The majority of these patients had an indication for hepatectomy but were ineligible for surgery due to insufficiency of the FLR. Radiation lobectomy was performed if the following inclusion criteria were met: (i) diagnosis of colorectal liver metastases (ii) requiring a major (>2 segments) hepatectomy (iii) insufficient FLR function on hepatobiliary iminodiacetic acid (HIDA) scan ( $\leq 2.7\%/min/m^2$ ), and (iv) contraindication for standard induction of FLR response (portal vein embolization), or radiation lobectomy deemed more appropriate after multidisciplinary deliberation. Exclusion criteria for radiation lobectomy were: (i) extrahepatic disease (excluding the primary tumor), and (ii) any contraindication precluding radioembolization or surgery. The following data were collected from patient records: demographics, clinical features such as Charlson Comorbidity (CCI) and Eastern Cooperative Oncology Group (ECOG) scores as well as systemic therapy regimen, mutation status, treatment information including segments targeted, pre- and post FLR function and average absorbed tumor dosage. Clinical response was determined through the RECIST 1.1 criteria on MRI images 2–3 months following radioembolization.<sup>16</sup> The UMC Utrecht Institutional Review Board approved the study. The need for informed consent was waived.

### Radioembolization/radiation lobectomy

Prior to the administration of the actual treatment dose, patients received a preparatory angiography to map the arterial anatomy of the liver, determine catheter-position(s) for scout dose injection and evaluate the risk of extrahepatic deposition of

radioactivity. The scout dose injected at preparatory angiography consisted of technetium-99m macroalbumin aggregates (<sup>99m</sup>Tc-MAA) in <sup>90</sup>Y glass-treated patients or <sup>166</sup>Ho scout microspheres in <sup>166</sup>Ho treated patients. If possible, injections were performed from a catheter position distal to any vessels that may cause extrahepatic deposition of microspheres. Otherwise, these vessels were coil-embolized. The prescribed activity was calculated using the Medical Internal Radiation Dose (MIRD) method. The target dose to the treated volume was 80–120 Gy for <sup>90</sup>Y and 60 Gy for <sup>166</sup>Ho. All patients received unilobar treatment with or without selective segmental targeting.

### Histological evaluation

Surgical pathology reports from included patients were reviewed, and all formalin-fixed, paraffin-embedded (FFPE) blocks with uniquely identified metastases were cut into 4-micron sections and stained with hematoxylin and eosin (H&E) in a Ventana Benchmark Ultra system. Response to treatment of individual metastases was scored using a regression grading system as described previously,<sup>17</sup> which takes into account the amount of therapy induced-fibrosis/necrosis in relation to the residual tumor. Briefly, ‘therapy-induced’ necrosis was defined as foci of stromal fibrinous exudates with collagen and fibroblasts, mucinous exudates (‘mucin lakes’) or necrosis with limited cellular debris. ‘Normal’ not therapy-induced necrosis (‘dirty necrosis’) was defined as cell detritus and inflammatory cells within the glandular lumina. Tumor regression grade 1 was defined as no residual tumor; 2 as few tumor cells scattered throughout the necrosis/fibrosis; 3 as residual cancer but predominant necrosis/fibrosis; 4 as predominance of residual tumor and 5 as no regression changes or only the presence of ‘dirty necrosis’. Next, regression grades 1 and 2 were classified as good responders, grade 3 and 4 as intermediate responders and grade 5 lesions as non-responders. Presence of tumor cells was based on morphology and GPA33+, CDX2+ and CK7- staining.

### Dosimetry

Dosimetry was performed using Simplicit<sup>90</sup>Y software version 2.4 (Mirada Medical Ltd.) and Q-Suite™ (Quirem Medical). Tumors and perfused volumes were delineated on pre-treatment portal phase contrast-enhanced CT images. These CT images were then manually registered to the CT images made alongside the post-treatment <sup>90</sup>Y PET/CT or <sup>166</sup>Ho SPECT/CT images. No volume restriction was applied. Accurate tumor-to-tumor registration was prioritized over liver contour registration in this process. Only manual rigid transformation i.e., translation and/or rotation of images, was performed. Absorbed dose for each lesion were subsequently calculated using the actual activity delivered (i.e., after deducting residual activity in administration material). Individual metastases were matched based on their segmental location on imaging as well as surgical and pathology reports (Fig. S1 for example case). When in doubt or when multiple metastases were close together, proximity to anatomical

landmarks (i.e., the falciform ligament, gallbladder, liver capsule, etc.) were additionally taken into consideration. One new metastasis was identified after radiation lobectomy; this lesion was excluded from further analysis.

### Immunohistochemistry

Immunohistochemical stainings were performed on 4-micron-thick FFPE sections mounted on a glass microscope slide. In short, after dewaxing and rehydration, endogenous peroxidase was blocked with 1.5% hydrogen peroxide in phosphate-buffered saline to prevent non-specific binding. Heat-mediated antigen retrieval was performed in either citrate pH 6 or ethylenediaminetetraacetic acid pH 8 (for CD45). Slides were incubated with primary antibody overnight at 4 °C, followed by incubation of 1 h with secondary antibody at room temperature. 3,3'-Diaminobenzidine was used as a chromogen and counterstaining was performed with hematoxylin. The following antibodies were used: GPA33 (Atlas [HPA018858]), CDX2 (Immunologic [ILM2353-C1]), CK7 (Biogenex [MU255-UC]), Ki-67 (BD Transduction Laboratories [610,959]), CAIX (Abcam [ab15086]), Olfm4 (Cell Signaling Technology [14,369]) and CD45 (Abcam [ab40763]).

### Computerized analysis

Stained slides were digitized using the NanoZoomer XR (Hamamatsu) scanner at  $\times 40$  magnification and stored in ndpi image format. Whole slide image analysis was performed using QuPath version 0.2.3.<sup>18</sup> Metastatic lesions were manually

annotated to allow further analysis of different regions of interest. Every unique cell within each region of interest was annotated and assigned a pixel threshold to allow classification of positive versus negative cells. For Ki-67, Olfm4 and CD45 a binary approach was used, while CAIX was given a H-score using three thresholds.<sup>19</sup> Next, a random forest supervised machine learning algorithm was interactively trained to distinguish tumor epithelial cells from all other cell detections (comprising mostly non-epithelial cells and radiation-induced fibrosis/necrosis).<sup>20</sup> Lastly, the number of positive tumor cells and tumor-infiltrating immune cells for each metastasis were extracted from the images and further analyzed in R (version 4.0.3). Fig. 1 summarizes the methodological setup. Metastases with a regression grade of 2 due to the presence of small clusters of tumor cells with interspersed ductular reactions (i.e., hyperplastic bile ducts) were excluded from further immunohistochemical analysis, as differentiation between these entities could not be made by the machine learning algorithm.

### Statistics

Summary statistics are given in mean or median  $\pm$  standard deviation (sd) or range to assess variability or standard error of the mean (sem) when comparing means, as indicated. If not stated otherwise, Welch's Two Sample *t* tests were used to compare means. Spearman's rank correlation coefficient ( $\rho$ ) was used to assess the association between variables, and corresponding *P*-values were computed via asymptotic *t* approximation.

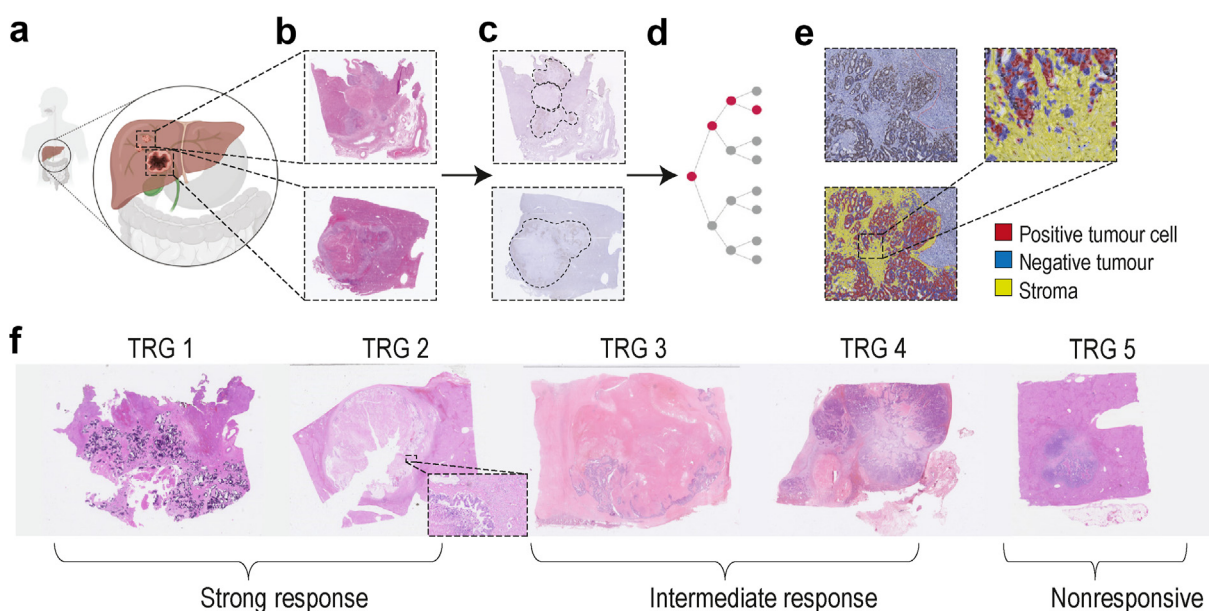


**Figure 1 Methodology** (a, b) Each unique macroscopically defined metastasis was selected from surgical pathology reports. (c) Stained slides were scanned and spatially distinct sub-lesions were delineated. (d, e) A random forest machine learning algorithm was interactively trained to accurately measure staining intensities of tumor cells. (f) Example of each TRG scored on H&E slides. TRG: Tumor Regression Grade

## Results

### Patient characteristics and treatment details

Seven patients with colorectal liver metastases underwent liver surgery after radioembolization. Patient and treatment characteristics are detailed in Table 1 and Table 2. Six patients had insufficient FLR as defined on HIDA scan, and received radioembolization to ablate the perfused lobe and induce hypertrophy of the future liver remnant (i.e., radiation lobectomy setting). One radiation segmentectomy was performed. The median age at date of diagnosis was  $55 \pm 11$  years. All patients received systemic therapy prior to radioembolization (the interval between systemic therapy and radioembolization was at least four weeks). Radioembolization was administered most often to the right lobe ( $n = 4$ ). Five patients received  $^{90}\text{Y}$  glass microspheres, two patients received  $^{166}\text{Ho}$  microspheres. The mean size of the largest metastasis prior to microsphere administration was  $3.7 \pm 1.0$  cm. Target lesions, measured according to RECIST 1.1 at 2–3 months following radioembolization/radiation lobectomy, were found to be responsive or stable in five cases.<sup>16</sup> Progressive disease was observed in two cases. One patient showed progressive disease with new lesions in the liver. The median time between radioembolization and surgery was 4 months, range 2.7–6.5 months.

### Radioembolization induces abnormal liver histology

All specimens showed pronounced radiation-induced changes, including fibrinous and mucinous exudates and necrosis (Fig. 2a). Microspheres in the tumor vascular bed and/or portal tracts were found in 85% of coupes, comprising all patients (Fig. 2b). Nevertheless, a strong response (regression grade  $\leq 2$ ) was found in all metastases where no microspheres could be found on microscopic evaluation. A common feature in radioembolized livers was ductular reactions (100% of patients), consisting of reactive bile ducts that proliferate in response to liver injury (Fig. 2d–f).<sup>21</sup> Ductular reactions could be

differentiated from small clusters of residual tumors by immunohistochemical confirmation of markers GPA33/CDX2 and CK7. In metastases that had residual cancer, 67% had outgrowth in the margin of the tumor (Figs. 2a and 3c). This morphology resembled the tumor outgrowth seen previously in radio-frequency ablated liver tumors,<sup>22</sup> or surrounding necrotic lesions induced by prolonged vascular clamping.<sup>23</sup>

### Heterogeneous response to radioembolization

For each metastasis ( $n = 27$ ), pathological response and matched average absorbed doses as defined on post-treatment imaging were determined (Fig. 3a).<sup>17</sup> Pathological response rates were satisfactory, with 52% (14/27) of metastases showing a strong response. Notably, patient A, the only KRAS mutated patient, had strong response in all three lesions (Fig. 3a, Table 1). Four patients (of seven total), had strong intertumor heterogeneity, with both strongly responding lesions as well as intermediate or unresponsive lesions (Fig. 3a, patient C, D, F, G). Moreover, in two patients we found intratumor heterogeneity, where lesions that received the same average dose had within-tumor regions with distinct response (Figs. 2g, 3b and 3c, patient C and F). No correlation was found between average absorbed dose and response in both  $^{90}\text{Y}$  ( $n = 16$  lesions,  $\rho = 0.093$ ,  $P = 0.73$ , Fig. 3b) or  $^{166}\text{Ho}$ -treated patients ( $n = 11$  lesions,  $\rho = 0.035$ ,  $P = 0.92$ , Fig. 3c). Moreover, there was no correlation between the response and the time between radioembolization and surgery ( $\rho = 0.075$ ,  $P = 0.71$ ).

### Nonresponsive cancer cells display features of tumor aggressiveness

A gradual increase in the percentage of proliferating cells was found with decreasing response ( $\rho = 0.56$ ,  $P = 0.014$ ) (Fig. 4a). Nonresponsive lesions frequently displayed large pools ( $>15\%$  of all tumor cells) of Olfm4 positive cells when compared to more strongly responding lesions (Fisher's exact test,  $P = 0.037$ ),

**Table 1** Patient characteristics

Patient	Age <sup>a</sup>	Sex	CCI <sup>a</sup>	ECOG <sup>a</sup>	Chemo <sup>b</sup>	Largest Lesion <sup>c</sup> (cm)	KRAS	RECIST 1.1	PFS <sup>d</sup> (days)	OS <sup>d</sup> (days)
A	59	Male	8	0	FOLFOXIRI-B	2.6	Mutated	S	324 <sup>e</sup>	880 <sup>e</sup>
B	50	Male	8	0	FOLFIRI-panitumumab	3.2	Wildtype	S	750 <sup>e</sup>	2136
C	59	Male	7	0	CAPOX-B	5.3	Wildtype	S	459 <sup>e</sup>	1,029 <sup>e</sup>
D	76	Male	10	1	FOLFOX-B	4.3	NA	PD	232 <sup>e</sup>	486 <sup>e</sup>
E	42	Female	6	0	FOLFIRI	4	Wildtype	PR	1,770 <sup>e</sup>	2255
F	55	Female	6	0	CAPOX-B	2.8	Wildtype	PD	1,134 <sup>e</sup>	1723
G	44	Male	6	0	CAPOX, FOLFOXIRI	NA	Wildtype	PR	1468	1468

CAP-OX-B: capecitabine, oxaliplatin, bevacizumab, CCI: charlson comorbidity index, CRC: colorectal carcinoma, ECOG: eastern cooperative oncology group, FOL-F-OX-IRI-B: folinic acid, fluorouracil, oxaliplatin, irinotecan, bevacizumab, PD: progressive disease, PFS: progression-free survival, PR: partial response, S: stable, OS: overall survival.

<sup>a</sup> At/from time of diagnosis of primary tumor.

<sup>b</sup> Interval between RE and chemotherapy was at least 4 weeks.

<sup>c</sup> Measured max. 3 months prior to RE.

<sup>d</sup> At/from time of diagnosis of liver metastases.

<sup>e</sup> Died or progressed.



**Table 2** Treatment details

Patient	Microsphere	Segments targeted	Dose <sup>a</sup> (Gy)	Pre-RL HIDA <sup>b</sup>	Post-RL HIDA <sup>b</sup>	Time (days) RL to		Surgery type
						FLR sufficiency	Surgery	
A	<sup>90</sup> Y	4–8	100	1	3	58	83	ERiL
B	<sup>90</sup> Y	4–8	80	0.8	2.2	91	123	ERiL
C	<sup>166</sup> Ho	4(b) - 8	60	1.3	2.7	75	89	RiL
D	<sup>90</sup> Y	1-4, 8	80	2.4	2.8	64	104	LL + S1 + S8
E	<sup>166</sup> Ho	5–8	60	2.4	2.6	167	199	RiL
F	<sup>90</sup> Y	2/3, 4	2/3 (100), 4 (150)	NA	NA	NA	128	Metastatectomy S2 and S5
G	<sup>90</sup> Y	2-5, 8	300	1.9	2.7	64	102	ELL

ELL: extended left lobectomy (E)LL (extended) left lobectomy (E)RiL: extended right lobectomy, HIDA: hepatobiliary scintigraphy, Ho: holmium, MIRD: medical internal radiation dose, RL: radiation lobectomy, Y: yttrium.

<sup>a</sup> Average prescribed dose to treated liver volume, calculated using MIRD method.

<sup>b</sup> In %/min/m<sup>2</sup>.

indicating the presence of radiation-insensitive cancer stem cells (Fig. 4b). High expression of hypoxia marker CAIX was found in strongly responding lesions compared to other lesions (H-score 150 in strongly responding lesions versus 44 in intermediate and nonresponsive lesions,  $P = 0.011$ , Fig. 4c). Despite the higher embolizing effect of <sup>166</sup>Ho microspheres, there was a trend towards increased hypoxia in <sup>90</sup>Y glass-treated tumors compared to <sup>166</sup>Ho (2.3-fold increase,  $P = 0.066$ , Fig. S2). Non-responsive lesions displayed larger influxes of tumor-infiltrating leukocytes compared with other lesions (3240 CD45 positive cells/mm<sup>2</sup> versus 650 cells/mm<sup>2</sup>), although this difference was not significant ( $P = 0.08$ ) (Fig. 4d).

## Discussion

In this pilot study, post-treatment resection samples of patients with colorectal liver metastases were studied to characterize tumor responses to radioembolization. A strong response was observed in 52% of metastases, but there was considerable heterogeneity between and within tumors. Immunohistochemical analysis revealed that non-responsive lesions were hyper-proliferative and maintained a large reservoir of cancer stem cells.

The latter was evidenced by the high frequency of Olfm4+ cells, which is a faithful marker of Lgr5-type stem cells, the the-facto stem cell of the intestinal crypt.<sup>24</sup> Lgr5+ cells were previously shown to be resistant to radiation and important for the regeneration of intestinal crypts after radiation exposure.<sup>25,26</sup> In addition, Lgr5+ cells serve as cancer stem cells in colorectal cancer and their selective ablation leads to tumor regression.<sup>14,15</sup> The presence of Lgr5+/Olfm4+ cells, whether pre-existing or therapy-induced, may be an important determinant of the radioembolization response, but may also represent a vulnerability. For example, selectively targeting of Lgr5+/Olfm4+ cells - for instance, using Lgr5 specific antibody–drug conjugates<sup>27</sup> - may sensitize patients to radioembolization.

Hypoxia is dogmatically considered to be one of the major factors negatively affecting the outcome of radiation therapy.<sup>12</sup> Somewhat unexpectedly, the current study found higher expression of hypoxia marker CAIX in strongly responsive lesions. This indicates that post-treatment hypoxia is mostly a matter of radiation-induced necrosis. Indeed, these strongly responding lesions represented metastases with small clusters of tumor cells scattered across necrotic fields. This also explains the paradoxical increased expression of CAIX in <sup>90</sup>Y compared to <sup>166</sup>Ho-treated tumors: although <sup>166</sup>Ho microspheres have a greater embolic effect, the <sup>90</sup>Y glass-treated group had more strongly responding lesions (Fig. S2). Thus, we surmise that the direct necrotic effect of radiation is a stronger driver of hypoxia than embolization of microspheres. Importantly, the hypoxic milieu induced by radiation in strongly responding lesions implies a double-edged sword: hypoxia induces the transcription of many genes with oncogenic function, including HIF1a and CAIX, which play a key role in tumor growth and progression.<sup>28,29</sup> As such, the radiation-induced hypoxic environment around these cancer cells can stimulate their expansion later on.

Radiation-induced DNA damage leads to cytosolic DNA, which is recognized by the cGas-STING pathway.<sup>13</sup> Subsequent activation of transcription factors IRF3 and NF-κB is thought to elicit an immune response.<sup>13</sup> Indeed, Craciun *et al.* found that radioembolization led to increased tumor-infiltrating leukocytes compared to transarterial chemoembolization or naïve controls in patients with hepatocellular carcinoma.<sup>30</sup> Similarly, Chew *et al.* explored radioembolization-induced immune activation by serial analysis of peripheral blood mononuclear cells and tumor tissues.<sup>31</sup> It was found that radioembolization induced an enrichment of natural killer cells, natural killer T cells and T cells, all of which have strong anti-tumor effect. Moreover, long-term response to radioembolization was associated with enrichment of bloodborne PD1- and Tim-3 expressing CD8+ T cells, CD4+ T cells and antigen-presenting cells.<sup>31</sup> Albeit not statistically significant, it is surprising that in the present study lower numbers

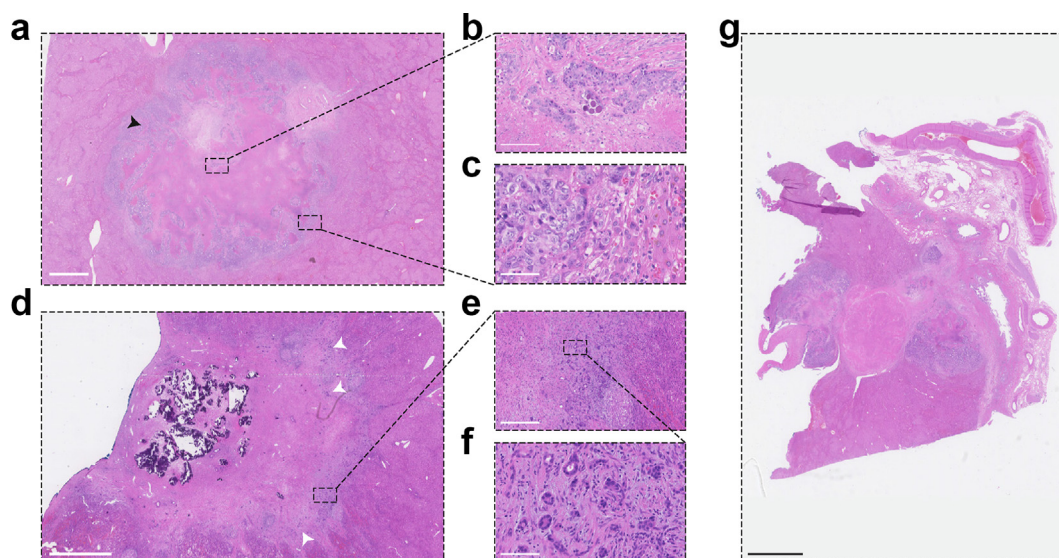


**Figure 2 Radioembolization induces aberrant morphology.** (a) Typical radiation-induced necrosis with viable tumor in the margin (black arrowhead). (b) Presence of microspheres within the necrotic center. (c) Zoom-in of tumor cells in the margin. (d, e) Presence of tumor clusters in the margin of the fibrosis (white arrowheads). (f) Zoom-in showing ductular reactions. (g) Example of spatially distinct sub-lesions within same pathological specimen. Scalebars (a–g): 2.5 mm, 100  $\mu$ m, 50  $\mu$ m, 2.5 mm, 500  $\mu$ m, 100  $\mu$ m, 5 mm

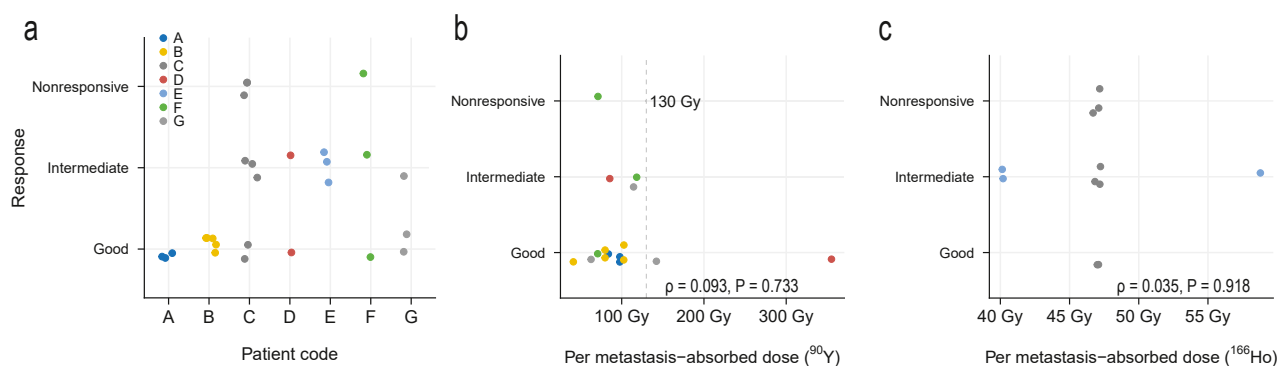


**Figure 3 Response to radioembolization is heterogeneous.** (a) Response for each metastasis ( $n = 27$ ) in each patient. Per metastasis-absorbed dose and response in patients treated with  $^{90}\text{Y}$  (b) ( $n = 16$  lesions) and  $^{166}\text{Ho}$  (c) ( $n = 11$  lesions). Color groups lesions from the same patient

of tumor-infiltrating cells (mean 650 cells/ $\text{mm}^2$ ) were found in strongly and moderately responding lesions, while high numbers were found in non-responsive lesions (3240 cells/ $\text{mm}^2$ ). This observed difference between studies could be explained by the difference in tumor type (hepatocellular carcinoma versus colorectal liver metastases). Indeed, Wang *et al.* report low numbers of tumor-infiltrating cells in post-treatment colorectal liver metastases.<sup>32</sup> We surmise that the reduced abundance of tumor-infiltrating cells observed in lesions with stronger tumor responses may be a result of the efficacy of the immune reaction and subsequent attenuation of immune influx. In this regard, the presence of apparently ineffective immune cells in non-responsive lesions may support the rationale of simultaneously

treating patients with immunotherapy to enhance the immune response. The feasibility of such approaches is exemplified by recent studies on the concomitant use of checkpoint inhibitors and radioembolization for unresectable non-colorectal hepatic metastases<sup>33</sup> and hepatocellular carcinoma.<sup>34,35</sup> For colorectal liver metastases data is still lacking, although a prospective study is underway.<sup>36</sup> Whether and which specific leukocytes influence the response to radioembolization in colorectal liver metastases remains to be explored, for example by comparing matched biopsies before and after treatment.

Most specimens had marked ductular reactions, consistent with a previous case series.<sup>37</sup> These are hyperplastic bile ducts arising from cholangiocyte- or hepatocyte precursors that

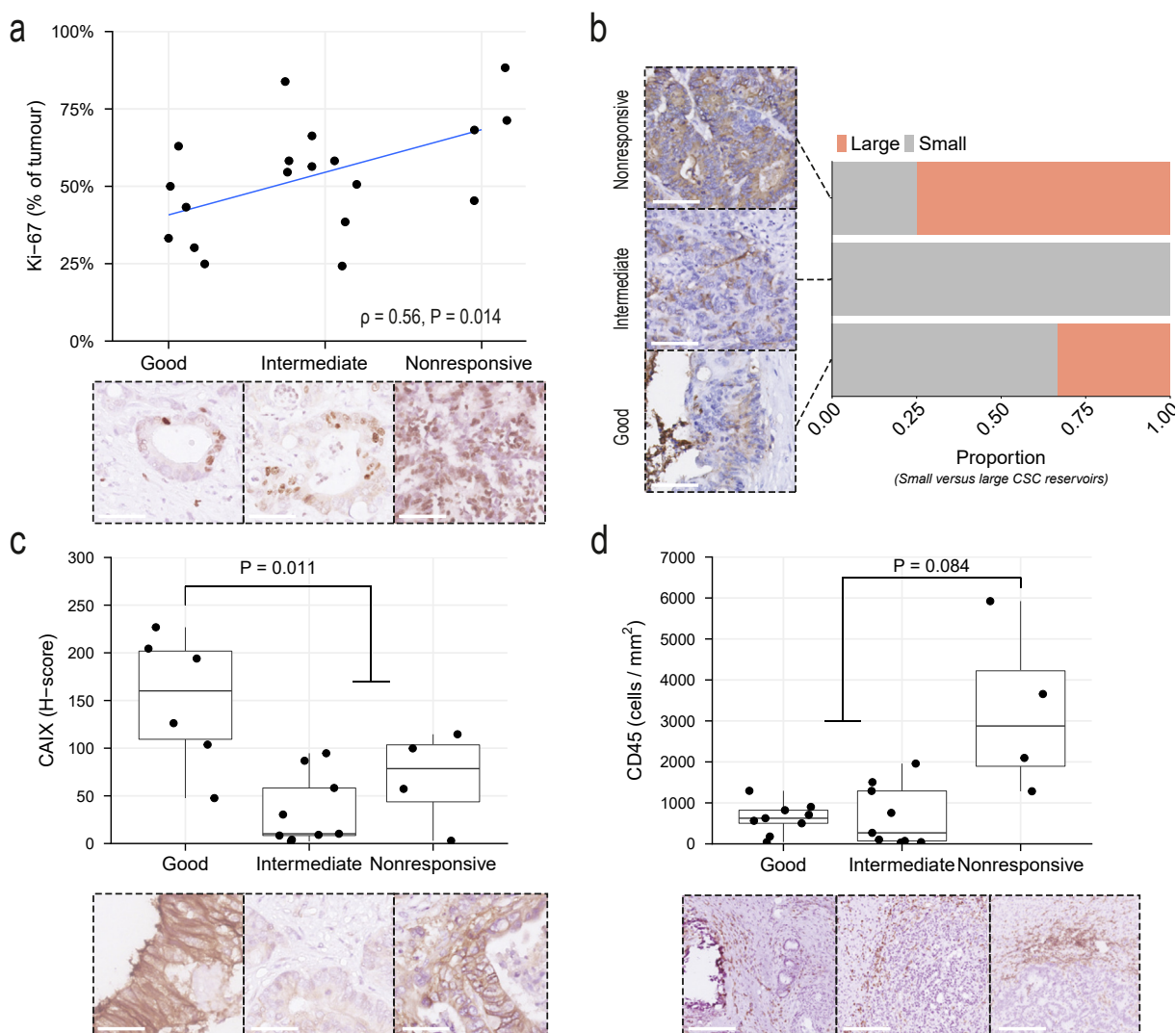


**Figure 4 Association between response and expression of markers of radiation-resistance.** (a) Association between response and proliferation marker Ki-67. (b) Proportion of metastases within each response group with either large (>15% of tumour cells) or small numbers of cancer stem cells (Olfm4+). (c) Association between response and hypoxia marker CAIX. (d) Association between pan-leukocyte marker CD45 and response. Representative stainings are depicted below each graph. Scalebars (a–c): 50  $\mu$ m, d: 500  $\mu$ m

respond to damaged livers.<sup>21</sup> Because of their irregular shape, heterogeneous nuclear size and lack of easily discernible lumina, they were often difficult to distinguish from tumor cells. The pathologist is advised to first verify the biliary nature of suspected tumorous clusters before ruling out a complete pathological response.

Limitations of this study include the small sample size, different microspheres used, and the semi-quantitative nature of immunohistochemical analysis, which was partially overcome by using a machine learning approach. Moreover, dosimetry is less accurate in small lesions, as is the case in this cohort of patients with colorectal liver metastases. This bias was partially corrected by prioritizing accurate tumor-to-tumor registration. However, the per metastasis dose represents an average dose across each

lesion, and intratumor response heterogeneity could additionally be influenced by microsphere distribution within the tumor. A subanalysis correlating the location of microspheres within each metastasis and within-metastases response could not be made due to the rarity of microspheres found within specimens. Furthermore, it should be noted that all patients included in the current study underwent systemic chemotherapy prior to radiation lobectomy, with a minimum interval of four weeks. As a result, it was not possible to make a definitive differentiation between necrosis induced by chemotherapy versus radiation. Finally, there was a large difference between patients regarding the time between radioembolization and surgery, although no correlation was found between time to surgery and tumor response.

Despite this study linking insufficient response to radiation lobectomy with pathological characteristics of therapy-surviving tumor cells, 52% of metastases exhibited a strong response.<sup>5</sup> This emphasizes the main advantage of radiation lobectomy for inducing FLR hypertrophy over portal venous embolization, which does not treat the tumor. This may be especially important for patients with hepatocellular carcinoma, where effective neoadjuvant therapies are currently unavailable. From a surgical perspective, this quality of radiation lobectomy allows for a “test-of-time” approach. While radiation lobectomy typically takes longer than portal venous embolization to induce FLR growth, this extra time can be utilized to monitor for the emergence of new lesions in the FLR or elsewhere, potentially avoiding unnecessary surgery. However, if this test-of-time approach benefits the patient is currently unknown, and future studies are needed to pinpoint the ideal timing between radiation lobectomy and surgical resection. For now, the aggressive nature of a subset of cancer cells with hyperproliferative, stem-cell like or hypoxic traits motivates rapid resection for patients in the radiation lobectomy setting.

In conclusion, previous studies have shown that baseline characteristics such as tumor differentiation, mutation status and tumor glycolysis<sup>7–11</sup> can influence tumor response. Future work may indicate whether the post-treatment phenotype observed in the current study is already present at baseline or whether it is radiation-induced. If pre-existing, pretreatment biopsies may be valuable for patient selection or pretreatment planning. The current study provides insights into the behavior of radioembolization-surviving cancer cells that may serve as a stepping stone for the use of concomitant therapies.

## Data availability statement

Research data will be shared upon reasonable request to the corresponding author.

## Funding

This research was supported by a private fund.

## Acknowledgements

The authors thank Domenico Castigliero and colleagues of the UMCU tissue facility for continuous support and Niek Peters, Esther Strating and Susanne van Schelven for scientific discussions and practical help.

## Conflict of interest statement

Marix Lam is a consultant for Boston Scientific and Terumo. Maarten Smits and Arthur Braat have served as speakers for SirTex, BTG, and Terumo. Ahmed Alsultan has served as a speaker for BTG. The Department of Radiology and Nuclear Medicine of the UMC Utrecht receives royalties from Quirem Medical. No other potential conflict of interest relevant to this article was reported.

## References

1. Tchelebi L, Sharma NK. (2019 May) Selective internal radiation therapy in the multidisciplinary management of liver metastases from colorectal carcinoma. *Semin Nucl Med* 49:182–188.
2. Gaba RC, Lewandowski RJ, Kulik LM, Riaz A, Ibrahim SM, Mulcahy MF *et al.* (2009 Jun 9) Radiation lobectomy: preliminary findings of hepatic volumetric response to lobar yttrium-90 radioembolization. *Ann Surg Oncol* 16:1587–1596.
3. Vouche M, Lewandowski RJ, Atassi R, Memon K, Gates VL, Ryu RK *et al.* (2013 Nov) Radiation lobectomy: time-dependent analysis of future liver remnant volume in unresectable liver cancer as a bridge to resection. *J Hepatol* 59:1029–1036.
4. Madoff DC, Gaba RC, Weber CN, Clark TWI, Saad WE. (2016 Feb) Portal venous interventions: state of the art. *Radiology* 278:333–353.
5. Boas FE, Bodei L, Sofocleous CT. (2017 Sep 1) Radioembolization of colorectal liver metastases: indications, technique, and outcomes. *J Nucl Med* 58(Supplement 2):104S–111S.
6. Bastiaannet R, Kappadath SC, Kunnen B, Braat AJAT, Lam MGEH, de Jong HWAM. (2018) The physics of radioembolization. *EJNMMI Phys* 5.
7. Dendy MS, Ludwig JM, Kokabi N, Stein SM, Lacy J, Hochster HS *et al.* (2018 Aug 21) Genomic mutations and histopathologic biomarkers in Y90 radioembolization for chemorefractory colorectal liver metastases. *Oncotarget* 9:32523–32533.
8. Lahti SJ, Xing M, Zhang D, Lee JJ, Magnetta MJ, Kim HS. (2015 Aug) KRAS status as an independent prognostic factor for survival after yttrium-90 radioembolization therapy for unresectable colorectal cancer liver metastases. *J Vasc Interv Radiol* 26:1102–1111.
9. van Roekel C, Jongen MJJ, Smits MLJ, Elias SG, Koopman M, Kranenburg O *et al.* (2020 Dec 22) Mode of progression after radioembolization in patients with colorectal cancer liver metastases. *EJNMMI Res* 10:107.
10. Kurilova I, Beets-Tan RGH, Flynn J, Gönen M, Ulaner G, Petre EN *et al.* (2019 Mar) Factors affecting oncologic outcomes of 90Y radioembolization of heavily pre-treated patients with colon cancer liver metastases. *Clin Colorectal Cancer* 18:8–18.
11. van den Hoven AF, Rosenbaum CENM, Elias SG, de Jong HWAM, Koopman M, Verkooijen HM *et al.* (2016 Jul) Insights into the dose–response relationship of radioembolization with resin <sup>90</sup>Y-microspheres: a prospective cohort study in patients with colorectal cancer liver metastases. *J Nucl Med* 57:1014–1019.
12. Sorensen BS, Horsman MR. (2020 Apr 21) Tumor hypoxia: impact on radiation therapy and molecular pathways. *Front Oncol*, 10.
13. Kwon J, Bakhoun SF. (2020 Jan) The cytosolic DNA-sensing cGAS–STING pathway in cancer. *Cancer Discov* 10:26–39.
14. de Sousa E Melo F, Kurtova Av, Harnoss JM, Kljavin N, Hoeck JD, Hung J *et al.* (2017) A distinct role for Lgr5 + stem cells in primary and metastatic colon cancer. *Nature [Internet]* 543:676–680. <https://doi.org/10.1038/nature21713>.
15. Shimokawa M, Ohta Y, Nishikori S, Matano M, Takano A, Fujii M *et al.* (2017) Visualization and targeting of LGR5 + human colon cancer stem cells. *Nature [Internet]* 545:187–192. <https://doi.org/10.1038/nature2081>.
16. Eisenhauer EA, Therasse P, Bogaerts J, Schwartz LH, Sargent D, Ford R *et al.* (2009) New response evaluation criteria in solid tumours:



- revised RECIST guideline (version 1.1). *Eur J Cancer [Internet]* 45: 228–247. <https://doi.org/10.1016/j.ejca.2008.10.026>.
17. Rubbia-Brandt L, Giostra E, Brezault C, Roth AD, Andres A, Audard V *et al.* (2007) Importance of histological tumor response assessment in predicting the outcome in patients with colorectal liver metastases treated with neo-adjuvant chemotherapy followed by liver surgery. *Annals of Oncology [Internet]* 18:299–304. <https://doi.org/10.1093/annonc/mdl386>.
  18. Bankhead P, Loughrey MB, Fernández JA, Dombrowski Y, McArt DG, Dunne PD *et al.* (2017) QuPath: open source software for digital pathology image analysis. *Sci Rep* 7:1–7.
  19. Hirsch FR, Varella-Garcia M, Bunn PA, di Maria MV, Veve R, Bremnes RM *et al.* (2003) Epidermal growth factor receptor in non-small-cell lung carcinomas: correlation between gene copy number and protein expression and impact on prognosis. *J Clin Oncol* 21: 3798–3807.
  20. Breiman L. (2001) Random forests. *Mach Learn* 45:5–32.
  21. Sato K, Marzioni M, Meng F, Francis H, Glaser S, Alpini G. (2019) Ductular reaction in liver diseases: pathological mechanisms and translational significances. *Hepatology* 69:420–430.
  22. Nijkamp MW, van der Bilt JDW, de Bruijn MT, Molenaar IQ, Voest EE, van Diest PJ *et al.* (2009 May) Accelerated perinecrotic outgrowth of colorectal liver metastases following radiofrequency ablation is a hypoxia-driven phenomenon. *Ann Surg* 249:814–823.
  23. van der Bilt JDW, Kranenburg O, Nijkamp MW, Smakman N, Veenendaal LM, te Velde EA *et al.* (2005 Jul) Ischemia/reperfusion accelerates the outgrowth of hepatic micrometastases in a highly standardized murine model. *Hepatology* 42:165–175.
  24. van der Flier LG, Haegebarth A, Stange DE, van de Wetering M, Clevers H. (2009) OLFM4 is a robust marker for stem cells in human intestine and marks a subset of colorectal cancer cells. *Gastroenterology [Internet]* 137: 15–17. <https://doi.org/10.1053/j.gastro.2009.05.035>.
  25. Hua G, Thin TH, Feldman R, Haimovitz-Friedman A, Clevers H, Fuks Z *et al.* (2012 Nov) Crypt base columnar stem cells in small intestines of mice are radioresistant. *Gastroenterology* 143:1266–1276.
  26. Metcalfe C, Kljavin NM, Ybarra R, de Sauvage FJ. (2014 Feb) Lgr5+ stem cells are indispensable for radiation-induced intestinal regeneration. *Cell Stem Cell* 14:149–159.
  27. Junttila MR, Mao W, Wang X, Wang BE, Pham T, Flygare J *et al.* (2015) Targeting LGR5+ cells with an antibody-drug conjugate for the treatment of colon cancer. *Sci Transl Med* 7:1–12.
  28. Chiche J, Ilc K, Laferrière J, Trottier E, Dayan F, Mazure NM *et al.* (2009 Jan 1) Hypoxia-inducible carbonic anhydrase IX and XII promote tumor cell growth by counteracting acidosis through the regulation of the intracellular pH. *Cancer Res* 69:358–368.
  29. Harris AL. (2002 Jan 1) Hypoxia — a key regulatory factor in tumour growth. *Nat Rev Cancer* 2:38–47.
  30. Craciun L, de Wind R, Demetter P, Lucidi V, Bohlok A, Michiels S *et al.* (2020 Dec 19) Retrospective analysis of the immunogenic effects of intra-arterial locoregional therapies in hepatocellular carcinoma: a rationale for combining selective internal radiation therapy (SIRT) and immunotherapy. *BMC Cancer* 20:135.
  31. Chew V, Lee YH, Pan L, Nasir NJM, Lim CJ, Chua C *et al.* (2019 Feb) Immune activation underlies a sustained clinical response to Yttrium-90 radioembolisation in hepatocellular carcinoma. *Gut* 68:335–346.
  32. Wang LM, Jani AR, Hill EJ, Sharma RA. (2013 Mar) Anatomical basis and histopathological changes resulting from selective internal radiotherapy for liver metastases. *J Clin Pathol* 66:205–211.
  33. Ruohoniemi DM, Zhan C, Wei J, Kulkarni K, Aaltonen ET, Horn JC *et al.* (2020 Aug) Safety and effectiveness of yttrium-90 radioembolization around the time of immune checkpoint inhibitors for unresectable hepatic metastases. *J Vasc Intervent Radiol* 31:1233–1241.
  34. Tai D, Loke K, Gogna A, Kaya NA, Tan SH, Hennedige T *et al.* (2021 Dec) Radioembolisation with Y90-resin microspheres followed by nivolumab for advanced hepatocellular carcinoma (CA 209-678): a single arm, single centre, phase 2 trial. *Lancet Gastroenterol Hepatol* 6: 1025–1035.
  35. Zhan C, Ruohoniemi D, Shanbhogue KP, Wei J, Welling TH, Gu P *et al.* (2020 Jan) Safety of combined yttrium-90 radioembolization and immune checkpoint inhibitor immunotherapy for hepatocellular carcinoma. *J Vasc Intervent Radiol* 31:25–34.
  36. Kasi PM, Toskich BM, Chandrasekharan C, Prabhakar D, Sharif S, Berg DJ *et al.* (2020 Feb 1) Immunotherapy with Y90-radioembolization for metastatic colorectal cancer (iRE-C). *J Clin Oncol* 38(suppl):TPS276. TPS276.
  37. Justinger C, Gruden J, Kouladouros K, Stravodimos C, Reimer P, Tannapfel A *et al.* (2018 Apr) Histopathological changes resulting from selective internal radiotherapy (SIRT). *J Surg Oncol* 117:1084–1091.

#### Appendix A. Supplementary data

Supplementary data to this article can be found online at <https://doi.org/10.1016/j.hpb.2023.06.011>.